

# Testbeam for the CMS ECAL upgrade for the High Luminosity phase of LHC

## Summer Student Report

18/06/2018 - 10/08/2018

**Group: EP-CMX/CMS**

Juan Salvador Tafoya Vargas (National Autonomous University of Mexico (UNAM), Mexico)

First Supervisor: Francesca Cavallari (National Institute for Nuclear Physics (INFN), Italy)

Second Supervisor: Riccardo Paramatti (National Institute for Nuclear Physics (INFN), Italy)

**Abstract:** With the incoming High Luminosity phase of LHC some upgrades for the CMS ECAL are in line. As a part of the characterization process, data was taken using either a laser as light source or electrons at the testbeam H4. Dependence of gain in terms of voltage and temperature were studied, which allowed later to compare the measurements obtained with the VFEs working at 120 MHz and 160 MHz. Additionally, the electron beam used for the test was studied after the characterization was done, allowing for a first reconstruction of energy.

### I. INTRODUCTION

Given the incoming increase in luminosity after the third long shutdown of LHC and the expected high pileup in CMS [1], it has become a priority to upgrade the current electronics to catch up with the higher luminosity. In the ECAL, particularly, most of these changes will be in VFE to increase the sampling time and improve both the temporal and energy resolution. The ECAL itself, made of lead tungstate scintillating crystals coupled with Avalanche Photodiodes (APD) for the read-out of the generated photons [2], will be kept during the upgrade. Since there is already a prototype for such modifications, tests are in order to characterize its behaviour, which also turns to be closely related with the particle used in such examinations.

During my stay at CERN as summer student, I joined the CMS ECAL upgrade test-beam at H4. There, I participated in the set-up, data-taking and data-analysis processes for carrying out such characterizations. Ahead, some of the tests are explained, as well as information obtained about the beam.

### II. APD GAIN

Of the two variables that affect the most the gain of the APD, voltage and temperature, the former is the easiest one to modify and possible the one with the greatest effect on it, specially due to the relatively constant temperature at the detectors area. Thus, it is first worth studying this behaviour.

With the gain defined by the APD output current as

$$G(V) = \frac{I_{\text{signal}}(V) - I_{\text{dark}}(V)}{I_{\text{signal}}(10 \text{ V}) - I_{\text{dark}}(10 \text{ V})} \quad (1)$$

and using the currents obtained from a voltage run using a laser as light source at 18 °C last year, the gain (represented as a black line in Figure 1) was computed. Furthermore, as it is chosen as a standard to operate with a gain of 50, for that very

same temperature a voltage of around 350 V is required. Thus, using data taken on H4 during the second week of internship for voltages over 320 V and renormalizing, the red curve in the same Figure was obtained and observed to follow closely the known pattern, with a slight difference due to not knowing the value of  $I_{\text{dark}}$ .

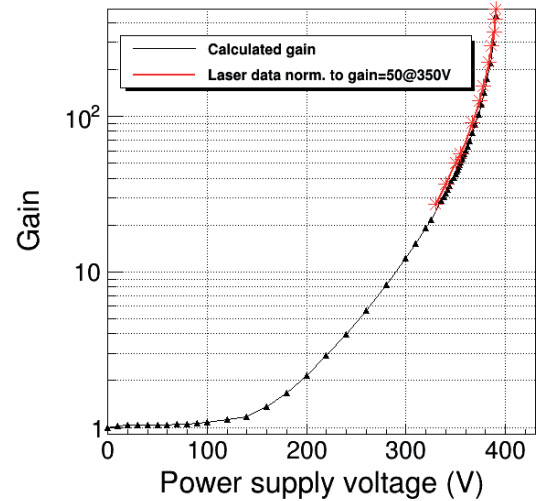


Figure 1. Comparison of the calculated gain of an APD with the response obtained while triggered by a laser and realising a voltage scan.

#### A. Gain vs Voltage fitting

As the exact voltage value may be slightly different for each APD, it is desired to know analytically the behaviour of the gain as a function of voltage. For such task, fitting the gain on plots such as the one shown in Figure 1 can give a pretty accurate description of it. Using Musienko's equation [3] given by

$$G(V) = \frac{a}{b} \left( e^{b(V_b - V)} - 1 \right) \quad (2)$$

where  $a$ ,  $b$  are constants and  $V_b$  is the breakdown voltage, it was possible to describe the plots for gains bigger than 10 ( $V > 300$  V) in voltage runs taken at 7.5, 10 and 18 °C (shown in Figure 2). Once the fitting has been done, finding the exact voltage value for which certain gains of interest are reached is easy. The voltages to have gains of 50, 100 and 200, as well as the fitting parameters are shown in Table 1.

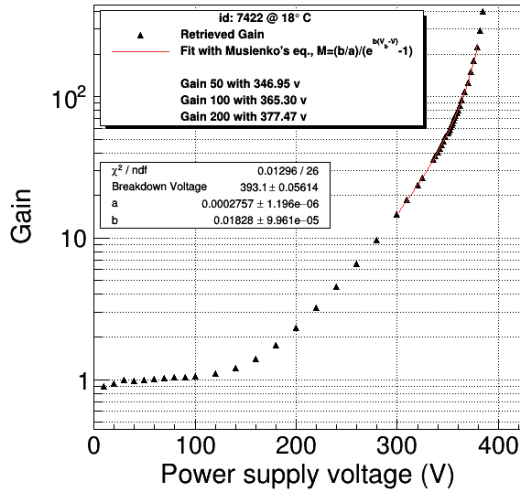


Figure 2. Fitting of the gain vs voltage dependance at 18 °C with Musienko's equation. Similar results were obtained at 10 °C and 7.5 °C.

	7.5 °C	10 °C	18 °C
$a (\times 10^{-4})$	2.775	2.739	2.757
$b (\times 10^{-2})$	1.900	1.908	1.828
$V(G = 50)$ [V]	338.68	340.31	346.95
$V(G = 100)$ [V]	356.63	358.35	365.30
$V(G = 200)$ [V]	368.59	370.39	377.47

Table 1. Fitting parameters with Musienko's equation (1) for the same APD at different temperatures.

Now that the voltages for the same gains at different temperatures are known, it arises the question, what if the temperature changes? Considering that the data sets used before were taken using the same APD, it is possible just to plot the values corresponding to gain 50, 100 and 200 in the same canvas for the 3 temperatures, and fit each with a linear function (as it is already known to behave as such). Figure 3 displays the fitting to the data and the parameters obtained for each set of points, describing how the voltage should change to compensate for variations in temperature. Since 18 °C is the value of reference, the fitting is re-written in such way that what matters is how far from this temperature the sensor is, and makes straightforward to see the operation voltage at that same temperature. Since for the ECAL the value of gain selected is 50, by measuring constantly the temperature around the detector it would be easy to correct for ambiantal fluctuations.

### III. TESTBEAM

During the last week of June, data was taken using the electron beam at the H4 testbeam in Prévessin with a 6x5 crystal array

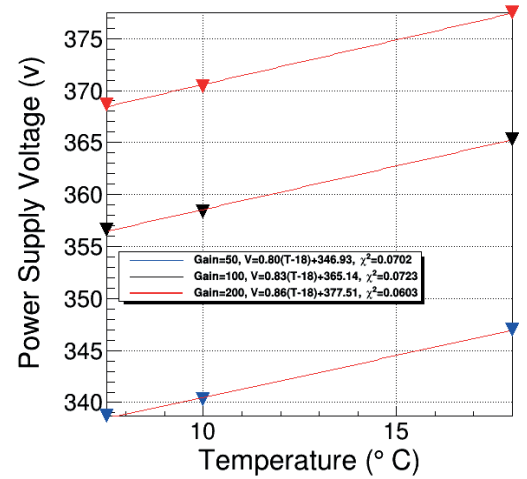


Figure 3. Voltage vs temp. dependence for keeping constant values of gain.

such as the one shown in the left side of Figure 4. Each of these crystals is a  $\text{PbWO}_4$  scintillator with an APD and its respective VFE attached to its back, and is identified by the names as shown in right side of the same Figure. For the tests, a collimated electron beam coming from the SPS was driven into the array after selecting a particular kinetic energy, which could have ranged from a few GeV to 200 GeV.

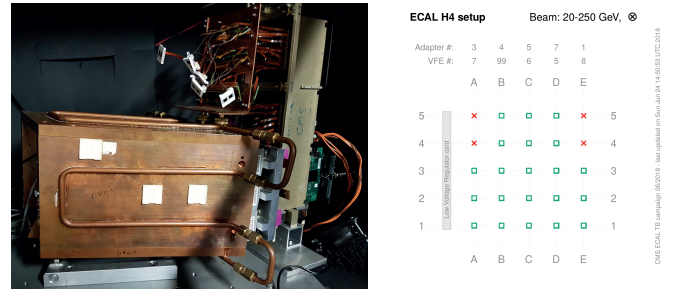


Figure 4. Left: side view of the ECAL 6x5 array used in H4. Right: ID of each crystal in the array.

The VFE at the test-beam are prototypes of the electronics that will be used in the HL-LHC phase. Particularly, ADCs at 120 MHz and 160 MHz are being tested to compare the energy resolution given by each.

#### A. Beam studies

Despite how well focused the beam could be, its propagation front cannot be considered as a punctual source. Instead, it follows a gaussian-like shape with most of the electrons moving very close to the beam axis, and fewer moving in the same direction but further from the center, creating a beam a couple of centimetres wide. This is exemplified in the Left side of Figure 5. As a consequence of this, just one crystal (with a face of  $2.5 \text{ cm} \times 2.5 \text{ cm}$ ) is not enough to contain all of the beam. Nevertheless, the solution for such effect is an easy one, as surrounding crystals are enough to capture most of the electrons. As displayed in the Right side of Figure 5, for a beam focused on the center of a crystal, this will contain approximately 80%, the lateral neighbors around 4%, and the

diagonal ones 1%. Further extensions of the considered zone, like combining the measurements of a  $5 \times 5$  area around the main target will improve the energy containment, but is unnecessary for demonstrative purposes.

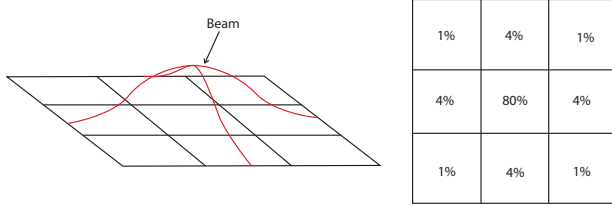


Figure 5. Left: shape representation of the beam propagation front. Right: containment ratios provided by the crystal array for a beam focused in the center of a crystal face.

Prior to the analysis of the beam, it is necessary to choose the electrons that will be taken into account. For that, it happens to be very helpful to watch at the beam shape given by the hodoscope. Since each scintillator fiber that composes the hodoscope registers the passing electrons and there are two sets of fibers arranged orthogonal to each other, the hodoscope gives a mapping of the beam, which allows to easily discard very dispersed electrons. Thus, in order to select a "clean" front of the beam, it was located the maximum of counts, and then selected the interval given by  $\pm 5$  of this value. For instance, as displayed in Figure 6 for a beam centered in C3, the maximum along the x-axis is located around  $-3$ , so the cuts (shown as red lines) enclose a pretty much clean section of the beam between  $-8$  and  $+2$ . This very same procedure was then repeated for the other axis, in this case the y-axis, and sets a working region.

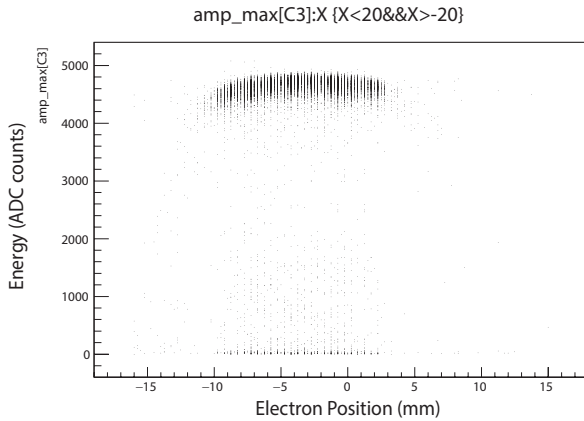


Figure 6. Hodoscope beam shaping along the X axis for a beam focused to the center of C3.

Retrieved from the VFE, Figure 7 shows the energy distribution of the detections from the crystals. The x-axis displays energy, while the y-axis shows the amount of particles counted for each energy. Before calibrating the energy for this data set, there are a couple of details that must be taken care of. On the far left of the plot, in the low energy side, there is a small tail that rises well above what could be considered to be noise. This corresponds to minimum ionizing particles, such as pions or muons, subproduct of the collimation that contaminates the beam. To the right of the electrons signal, on the high energy side, seamlessly random counts appear to

even double the value of the global maximum. This counts correspond to spikes, direct hits of particles into the APD that trigger a fastest and more intense signal.

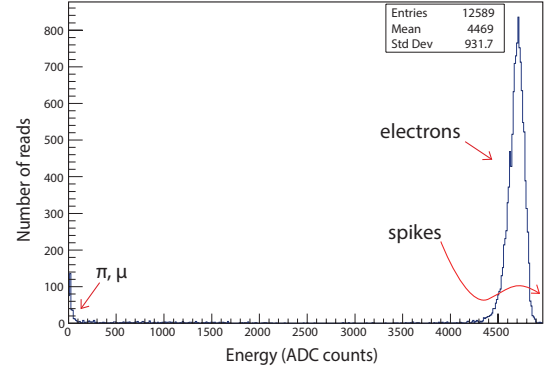


Figure 7. Entire energy spectrum, displaying the signal corresponding to the electrons of the beam, as well as contaminating  $\mu$  and  $\pi$ , and high energy spikes.

As a first approximation, just discarding the events under half of the weighted mean of the plot is enough to take out most of the contaminating particles, while  $\text{mean} + 300$  would remove most of the spikes. Figure 8 displays a cleaner section of the same data set as before, containing mostly only the events generated by electrons. This section allows already for a first fitting.

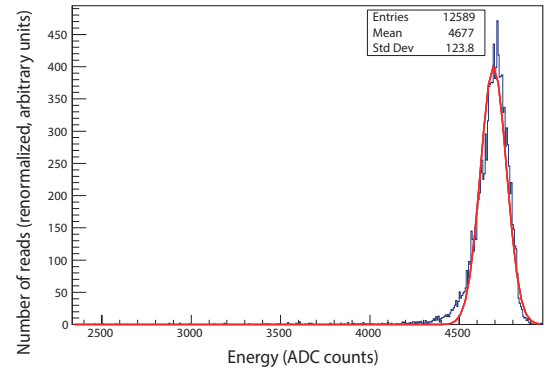


Figure 8. Trimmed energy spectrum section containing almost only electrons, as well as a first gaussian fitting around the peak.

Knowing that the signal given by the electrons should follow a crystalball shape, it becomes easy to define a general rule for the selection of events after realizing a first fitting with a gaussian only around the main peak:

- Everything under the center of the gaussian  $- 10\sigma$  (both parameters obtained from the fitting) is outside of the exponential tail, so it can be considered as contaminating particles
- Anything above  $\text{mean} + 5\sigma$  is outside of the gaussian tail, so it can be considered as high energy spikes

Thus, it becomes of interest to know what ratio of the beam is composed by electrons, namely the purity of the beam, that can be defined as

$$purity = \frac{\#_{tot\ events} - \#_{\pi,\mu} - \#_{spikes}}{\#_{tot\ events}} \quad (3)$$

where the symbol  $\#$  corresponds to the number of counts (or events) in each interval. Figure 9 displays the behaviour of the purity when changing the energy of the beam from 25 GeV to 200 GeV at 8.5 °C using the 120 MHz ADC. These purity calculations were made for beams directed at the crystals C2, C3 and C4. Similarly, a spike ratio study was done using the value of  $\#_{spikes}/\#_{tot\ events}$ , and is displayed in Figure 10.

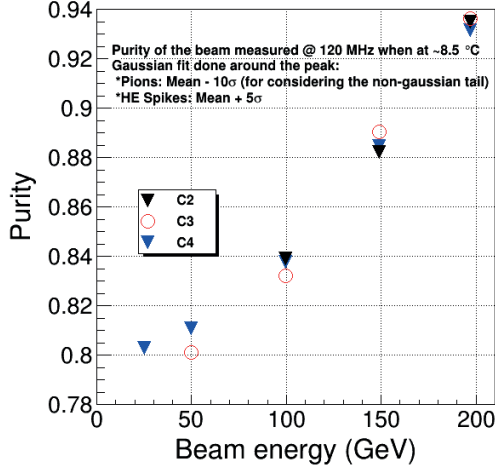


Figure 9. Purity of the beam calculated from the crystals C2, C3 and C4 at 8.5 °C.

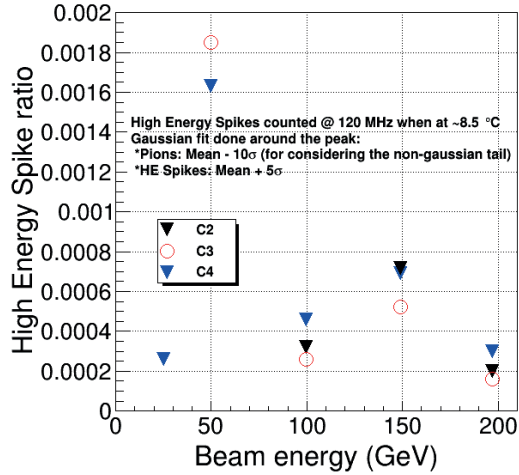


Figure 10. High energy spike ratio measured at 8.5 °C.

### B. Further gain study

As it has already been mentioned, it is of extreme importance to know the behaviour of the gain as a function of temperature. Previously this was briefly studied for the APD alone, but the scintillator's light yield also changes with temperature. Thus, as the response of the whole system is the principal interest, it was necessary to analyse the behaviour when the source of photons was the scintillator.

Taking advantage of the availability of the beam and the planned tests at low temperature, several runs were taken while the testbeam was chilled from 18 °C to 7 °C using a 100 GeV. Knowing beforehand that the temperature dependence of the gain is linear, the measurements were normalized such that the gain of the APD+Crystal system at 18 °C is 50 (since the voltage, of around 355 V for each APD, was not modified in the process). Combining with data taken on a different temperature ramp, it was possible to also compare the response of the 120 MHz and 160 MHz as shown in Figure 11 for various crystals. In addition to the collective response of the detector, data was also taken with a lower voltage set so that the APD gain was around 50 at the time of measurement, thereafter any change in the gain would be produced solely by the crystal (it is displayed as the light blue line in the plot).

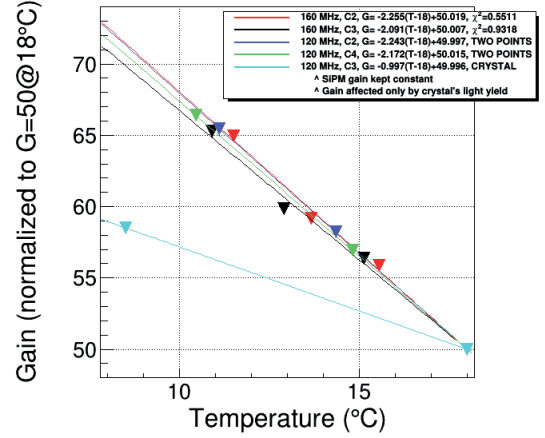


Figure 11. APD and crystal light yield dependance on temperature.

By looking at the fitting functions obtained, various things can be quickly noted. First of all, there is not a clear improvement when using either the 120 MHz or 160 MHz electronics, the response stays almost the same. Now, from comparing the slope of the fitting for the APD+crystal system (about -2) and of the crystal (about -1), it is easy to notice that for each degree that the temperature changes, there is a change of the global gain by 2 units: 1 given by the change of light output of the crystal, and 1 for the change in gain of the APD. So, while it is desired to keep the gain as constant as possible at a value of 50, a decrease of temperature of 1 °C would increase the production of photons by  $\sim 2\%$  and improve the APD gain by also  $\sim 2\%$ . This is consistent with expectations.

### C. Energy reconstruction

Given small difference in the manufacturing process, the APDs have slightly different responses to the same voltage. To compensate for that, it is necessary to find an intercalibration factor that would allow to compare the measurements given by different photodiodes. Defining such factor as

$$C_i = \frac{0.796 \times E_{beam}}{mean_{fit,i}} \quad (4)$$

where  $E_{beam}$  is the energy of the beam irradiating the  $i$ -th crystal and 0.796 is the energy contained in the central crystal

according to Monte Carlo simulations, the calculation becomes trivial. Using a run over all the crystals with a 150 GeV beam at 18 °C and the method previously described to fit the curve, the intercalibration factors shown in Figure 12 were obtained.

	A	B	C	D	E	
5	✗	0.0238	0.0317	0.0301	✗	5
4	✗	0.0227	0.0240	0.0242	✗	4
3	0.0245	0.0232	0.0254	0.0237	0.0225	3
2	0.0213	0.0208	0.0220	0.0229	0.0197	2
1	0.0209	0.0209	0.0222	0.0256	0.0205	1
	A	B	C	D	E	

Figure 12. Intercalibration factors at 18 °C.

Now that it is possible to combine the information of each crystal, reconstructing the energy of the beam is as easy as making the weighted sum

$$E_{3 \times 3} = \sum_{i=1}^9 C_i \times mean_i \quad (5)$$

which would consider the measurements over the main crystal of interaction, and the immediate neighbors of it. For instance, for a 150 GeV beam centered in B2, the energy recorded by each of the crystals was as shown in Figure 13, where also the corresponding percentage measured energy is displayed for each one. For this particular case, the total energy recovered from the array was 141.75 GeV, which is about the expected considering that more surrounding crystals could increase that value due to high dispersion electrons.

	A	B	C	
3	1.423 1.00%	4.951 3.49%	0.586 (GeV) 0.41%	3
2	3.476 2.45%	118.987 83.94%	4.977 (GeV) 3.51%	2
1	1.236 0.82%	4.288 3.02%	1.835 (GeV) 1.29%	1
	A	B	C	

Figure 13. Energy reconstruction for a 150 GeV beam centered in B2.

#### IV. CONCLUSIONS

Given the results obtained after the data analysis, the prototype of the ECAL VFE shows very favourable results operating at either 120 MHz or 160 MHz. Further analysis would allow to decide if the fastest of both electronics has a considerable advantage over the other given the limitations set by the available data transfer rates.

As a summer student, during my time at CERN I got the chance to participate in all the processes of the data taking and analysis, a rare event given the short length of the internship. It was a unique opportunity to be able to work side by side with experts of the area, and an invaluable learning experience all the way through.

#### REFERENCES

- [1] CMS Collaboration, *CMS Conference Report - Precision Crystal Calorimetry at High Energy and High Luminosity CMS ECAL Performance at 13 TeV and Upgrade Test Beam studies*, Geneva, Switzerland: CERN, 2016.
- [2] ECAL Group, CMS Collaboration, *CMS Conference Report - A Pedagogical Introduction to the CMS Electromagnetic Calorimeter*, Geneva, Switzerland: CERN, 1998.
- [3] IEEE/NPSS Radiation Effects Committee, *1999 IEEE NSREC - Nuclear and Space Radiation Effects Conference. Short Course*, Virginia, USA: IEEE, 1999.